Identification of interactive molecules between antler stem cells and dermal papilla cells using an in vitro co-culture system

Hongmei Sun, Zhigang Sui, Datao Wang, Hengxing Ba, Haiping Zhao, Lihua Zhang & Chunyi Li

Journal of Molecular Histology

ISSN 1567-2379

J Mol Hist DOI 10.1007/s10735-019-09853-9





Your article is protected by copyright and all rights are held exclusively by Springer Nature B.V.. This e-offprint is for personal use only and shall not be self-archived in electronic repositories. If you wish to self-archive your article, please use the accepted manuscript version for posting on your own website. You may further deposit the accepted manuscript version in any repository, provided it is only made publicly available 12 months after official publication or later and provided acknowledgement is given to the original source of publication and a link is inserted to the published article on Springer's website. The link must be accompanied by the following text: "The final publication is available at link.springer.com".



Journal of Molecular Histology https://doi.org/10.1007/s10735-019-09853-9

ORIGINAL PAPER



Identification of interactive molecules between antler stem cells and dermal papilla cells using an in vitro co-culture system

Hongmei Sun¹ · Zhigang Sui² · Datao Wang¹ · Hengxing Ba¹ · Haiping Zhao¹ · Lihua Zhang² · Chunyi Li^{1,3}

Received: 13 October 2019 / Accepted: 30 November 2019 © Springer Nature B.V. 2019

Abstract

Deer antlers are the only mammalian organs capable of complete renewal. Antler renewal is a stem cell-based [antler stem cells (ASCs)] process. Maintenance and activation of the ASCs require them to be located in a specialized microenvironment (niche), and to interact with the cells resident in the niche. Based on previous experiments we found that niche of the ASCs is provided by the closely associated enveloping skin, which currently was known includes dermal papilla cells (DPCs) and epidermal cells. Antler generation/regeneration are triggered by the interactions between ASCs and the niche. In the present study, we established an in vitro co-culture system in which ASCs and DPCs, were cultured together to mimic the in vivo state. A MLEFF strategy was adopted to identify the interactive molecules from the co-culture system. In total, 128 molecules were identified and over 60% belonged to exosomes. Important biological processes that were activated by these molecules included osteoblast differentiation, angiogenesis, and the PI3K-AKT signaling pathway. In so doing, we have significantly simplified the process for identifying interactive molecules, which may be the key signals for triggering antler formation/renewal. Further study of these molecules will help us to gain insights into the mechanism of mammalian organ regeneration.

Keywords Deer antler · Stem cell · Stem cell niche · Proteomics · Regeneration

Abbreviations

ASC Antler stem cell
DP Dermal papilla
DPC Dermal papilla cell
RT Room temperature

Hongmei Sun and Zhigang Sui have contributed equally to this work.

- ☐ Chunyi Li lichunyi1959@163.com

Hongmei Sun sunhongmei@caas.cn

Zhigang Sui zhigangsui16@163.com

Published online: 19 December 2019

- ¹ Institute of Special Animal and Plant Sciences, Chinese Academy of Agricultural Sciences, Changchun, China
- ² Key Laboratory of Separation Science for Analytical Chemistry, National Chromatographic R. & A. Center, Dalian Institute of Chemical Physics, Chinese Academy of Science, Dalian, China
- ³ Changchun Sci-Tech University, Changchun, China

SILAC Stable isotope labelling of amino acids

CM Condition media LiCl Lithium chloride

AP Antlerogenic periosteum PP Pedicle periosteum

Introduction

Organ regeneration is the "holy grail" of modern regenerative medicine. To realize this dream, regenerative medicine must be supported by determining the mechanisms of regeneration through investigating different animal model systems (Li et al. 2009b). Among these systems, deer antler stands out as the only mammalian appendage capable of complete annual renewal. Therefore, it offers a unique opportunity to explore how nature has solved the problem of regeneration of a complex mammalian organ including bone, cartilage, blood vessels, nerves and full thickness of skin (Goss 1995).

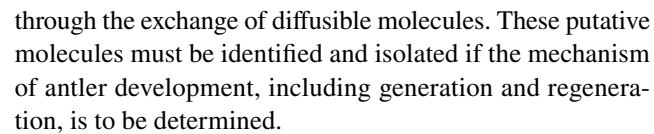
Antlers are deer cranial appendages that are cast and fully regenerate from the permanent frontal bony protuberances, known as pedicles, in yearly cycles (Li et al. 2005). It is known that antler regeneration relies on the cells resident in the pedicle periosteum (PP) (Li et al. 2007); and deer



pedicles and the first antlers are initially derived from the antlerogenic periosteum (AP), which overlies the frontal crest in a prepubertal male deer. Deletion of the AP abrogates future antler development and transplantation of the AP elsewhere on the deer body induces ectopic antler formation (Goss and Powel 1985; H and J 1974; Li and Suttie 2003). Our recent studies showed that the AP cells possess partial characteristics of embryonic stem cells, such as (i) expressing key embryonic stem cell markers Oct4, Sox2, Nanog, CD9, telomerase and nucleostemin; and (ii) being multipotent as they could be readily induced to differentiate into chondroblasts, adipocytes, myoblasts and neuronal-like cells (Harper et al. 2009; Rolf et al. 2008). Consequently, these cells are called "antler stem cells (ASCs)" (Li et al. 2009b).

Maintenance and activation of stem cells require them to be located in a specialized microenvironment, and to interact with the cells resident in the niche. The stem cell niche is highly dynamic with multiple opportunities for intervention, and stimulates proliferation and differentiation of stem cells, or causes reversion of differentiated cells to stem cells (Chunyi Li et al. 2011). Likewise, the ASCs, as a type of stem cells, must also reside in and interact with their niche. Based on our previous experiments of heterotopic grafting and intradermal transplantation, we found that skin epidermis and hair follicles were essential in activating initial antler generation(Li and Suttie 2000; Li et al. 2007, 2008). So, the covering skin must have constituted a main component of the ASC niche. Further research found that among the cell types resident in the skin, the most likely candidates that participated in the interaction with the ASCs are dermal papilla cells (DPCs) and epidermal cells (Li et al. 2009a, Li et al. 2010; RJ 1987).

It is reported that two main interactive processes, induction and feedback, are possibly involved in initial antler generation or regeneration (Li and Suttie 2000). In brief, the ASCs release signaling molecules, and these molecules diffuse through the overlying fibrous layer, compressed subcutaneous loose connective tissue and its attached inner part of dermis and finally reach and act on the dermal papilla cells (DPCs) of a hair follicle (induction) (Li et al. 2009a). The stimulated DPCs exert their influence via both paracrine and juxtacrine mechanisms on the overlying epidermis (angled and thick hair shaft, mono-lobed sebaceous glands, presence of sweat glands), which is then transformed into antler velvet (vertical and thin hair shaft, large multi-lobed sebaceous glands, absence of sweat glands and thickened epidermis). In turn, signals are received by the DPCs from the thickened epidermis via both paracrine and juxtacrine mechanisms (feedback). Subsequently, the DPCs secrete feedback molecules, which directly act on the ASCs and stimulate them to rapidly proliferate and differentiate and thus form an antler (Li et al. 2009b). Therefore, these interactions are achieved



Due to the complexity of the in vivo ASC niche and the likely low abundance of the interactive molecules, it would be a formidable, if not impossible, task to identify and isolate these molecules in vivo. Therefore, we recently established an in vitro co-culture system in which all the identified interactive cell types were placed together to maximally mimic the in vivo situation. In doing so, an approach to identify the putative interactive molecules was effectively simplified.

Furthermore, A MLEFF strategy including stable isotope labelling of amino acids in culture (SILAC) was adopted to pinpoint proteins that were synthesized and secreted only during co-culture, which greatly facilitated the identification of putative interactive molecules from the background noise through mass spectrometry analysis. Moreover, SILAC has the advantage of being able to mix samples at the beginning to reduce sample-to-sample variability. The identification and isolation of these molecules will not only enhance our knowledge of antler development, but also provide significant impacts for regenerative medicine in general.

The aims of the present study were to (1) establish a unique in vitro cell co-culture system that could maximally mimic the in vivo state to allow interactions between the ASCs and DPCs from the niche to take place; (2) identify the differentially expressed SILAC-labelled proteins in the co-culture system using mass-spectrometry; (3) analyze the identified molecules and activated transduction pathways to gain insights into the molecular mechanisms underlying antler generation/regeneration.

Materials and methods

Ethics statement

All animals were handled in strict accordance with good animal practice according to the Animal Ethics Procedures and Guidelines of the People's Republic of China, and the study was approved by The Animal Administration and Ethics Committee of Institute of Special Animal and Plant Sciences, Chinese Academy of Agricultural Sciences (Permit Number: ISAPSAEC-2018-018).

Cell culture

AP and skin were obtained from three heads of 6-monthold male sika deer calves as described previously by Li and Suttie. AP cells (now called ASCs) were cultured as described previously (Li 2012) in DMEM (Life, USA) plus



10% FBS (Gibco, USA), 100 U/ml penicillin and 100 μg/ml streptomycin (Invitrogen, USA) at 37 °C in 5% CO2. Cells were passaged using trypsin (Sigma, USA) and stored in liquid nitrogen in freezing medium (FBS +10% DMSO). Detailed procedures for primary ASC culture have been described elsewhere (Sun et al. 2012). DPCs were cultured by the method of microdissection. The sampled skin was washed with DMEM containing 500 U/ml penicillin and 500 g/ml streptomycin. The skin was sliced at 0.7 mm in thickness along the longitudinal orientation of resident hair shafts again using our patented cutter (Patent No: ZL2014 2 0335401.8). To facilitate the isolation of hair follicles from skin slices, the dermal tissue above and under the hair bulb zone was removed using a scalpel. Microdissection was performed under a stereomicroscope to locate and isolate these follicles. Each isolated follicle was transferred into a 10 cm dish containing digestion medium (DMEM+50 U/ ml collagenase + 5% FBS + 100 U/ml penicillin + 100 g/ml streptomycin) at room temperature (RT). After 2–3 h, the dermal papillas (DPs) were isolated from the follicles under the stereomicroscope and were seeded into 3.5 cm dishes and cultured in a humidified incubator at 37°C and 5% CO₂ for 4-6 days in the DMEM medium containing 10% FBS and 10% deer serum. Cells were harvested by trypsinization and seeded into a T25 flask and collected and stored frozen as for the ASCs.

Immunochemical localization

The DPCs at a density of 1×10^4 cells/well were seeded in 24-well plates for 24 h. For immunochemical localization, the medium was discarded, and the cells were fixed in 10% formalin. The fixed cells were then pretreated with 3% H_2O_2 to inactivate the intrinsic peroxidase after washing three times in PBS, incubated with the primary polyclonal antibodies [rabbit anti-vimentin (1:1000), VEGF (1:1000) or SMA- α (1:2000)] respectively at 4 °C overnight. The cells were then incubated with the fluorescently-labeled goat anti-rabbit secondary antibody for 2 h at RT and examined using an inverted fluorescent microscope (Leica DMI4000B) (Rufaut et al. 2013).

Reaction of DPCs to lithium chloride (LiCl) in nodule size

DPCs were prepared by culturing in T75 flasks as above. Cells were harvested by trypsinization, resuspended in culture medium, and seed into a 6-well plate at a density of 1.2×10^6 cells/well. LiCl was then added at the concentration of 0, 10, 20, 30 mM, respectively. Cells were maintained in 2.0 ml/well medium and half-volume of medium was replaced with fresh medium at every second day. Assays were stopped once spheroid cell aggregates were properly

formed (around 1–2 weeks). Cell aggregates/nodules were photographed and their diameters measured using the image analysis software (Image J).

Staining of endogenous alkaline phosphatase and versican in the DPC nodules

Staining of alkaline phosphatase and the versican in the DPC nodules was carried out respectively. For the former, BCIP/NBT Alkaline Phosphatase Color Development KIT (Beyotime, Jiangsu, china) was adopted following the manufacturer's instruction. Briefly, nodules were fixed in 10% formalin for 30 min at room temperature. The fixed DPC nodules were then washed three times in PBS for 5 min, incubated with BCIP/NBT color solution at RT for 30 min, and examined using an inverted microscope (Leica DMI4000B). For the latter, Immunofluorescent staining method was adopted with anti-versican antibody (Rb a versican/RBITC, bs-2533R-RBITC, Shanghai Bioss, 1:200).

Establishment of co-culture system

ASCs and DPCs were cultured as above then trypsinized and centrifuged to remove trypsin, and resuspended in the culture medium at a density of 1.0×10^5 cells/ml and 1.2×10^6 cells/ml respectively. The ASC suspension (0.5 ml) was gently seeded onto the membrane of each inverted transwellinsert of a 6-well-plate. The inverted inserts were transferred to a 10 cm culture dish and a few PBS droplets were added surrounding the inserts for maintaining humidity. The dish was placed in a humidified incubator at 37 °C, 5% CO₂ for 3 h. Thereafter, the inserts were re-inverted and put back into the original well in the 6-well-transwell-plate containing 2.6 ml culture medium/well. The DPC suspension (1.5 ml) was then seeded into each of the inserts, the cells allowed to precipitate onto the insert membrane, and the plates incubated at 37 °C and 5% CO₂ for 7-12 days. For the ASCs or DPCs singular cultures, the method was the same as the aforementioned procedure, except only one cell type was seeded on one side of the insert membrane.

RT-qPCR

To determine the expression levels of Nanog, Klf-4 and DKK3 genes from both the co-cultured and the ASC singular-cultured groups, RT-qPCR was performed using a SYBR primescript RT-PCR Kit (TaKaRa, Dalian, China). Total RNA was isolated from the ASCs using Trizol extraction kit and purified on a silica base spin column (SK1321, Shanghai Shenggong Inc, China) according to manufacturer's protocol. Primers were designed using the software of primer5 (Nanog ps: Forward primer: CCAGCCTTGGAACAATCA GT, Reverse primer: GTTTGGGAATAAATCCGTGAAT;



Klf4: Forward primer: CTGGAGAGTGGAGGAGTCGG, Reverse primer: TCCTGATGGGACAGCGAGTT; Dkk3: Forward primer: AAAAAGTTGGCATGCAGCG, Reverse primer: TCAACCTCGCGGAACATCTC).

SILAC analysis

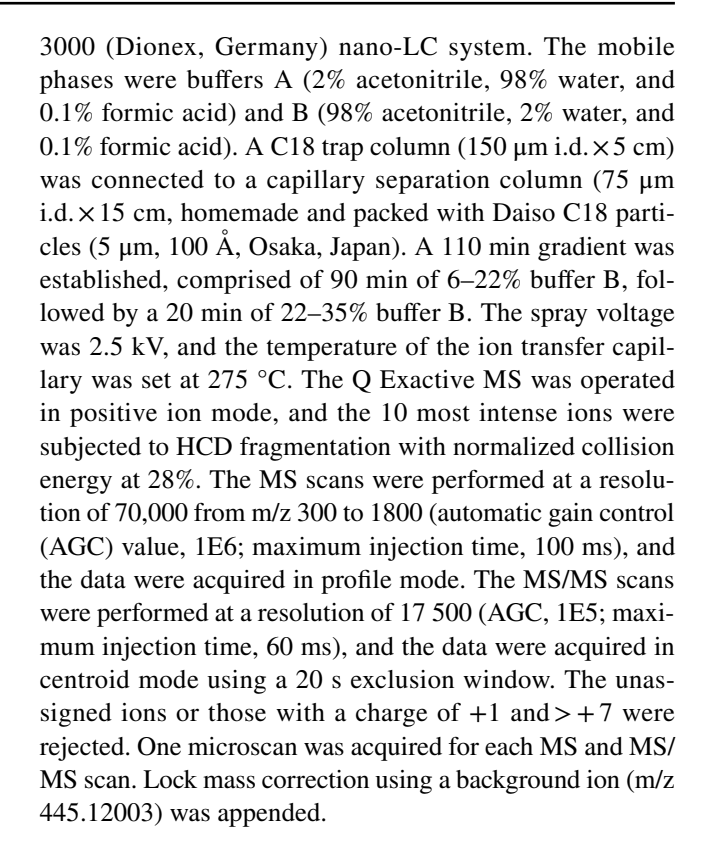
Both the ASCs and DPCs was split into two flasks separately: one containing "medium" labeling media and the other "heavy" labeling media (Pierce SILAC Protein Quantitation Kits, Thermo, USA). For the "medium" labeling media (Lys-4), L-lysine- and L-arginine-depleted SILAC DMEM media were supplemented with [4,4,5,5-D4] L-lysine (100 µg/ml) and L-arginine (100 µg/ml), 10% dialyzed fetal bovine serum (FBS), and a 1% penicillin/streptomycin mixture. For the "heavy" labeling media (Lys-8), only [4,4,5,5-D4] L-lysine was replaced with [13C6, 15N2] L-lysine. Each cell type and in each type of media ("medium" or "heavy") was continuously passaged for seven doubling times with approximately every 2-3 days per passage. At this stage, incorporation of labeling amino acid into cells should be over 95% based on the kit description. The cells in the "medium" media were continuously cultured; whereas, the cells (ASCs and DPCs) in the "heavy" media were co-cultured (as describing above).

Protein preparation

Condition media (CM) from each culture was collected into 50 ml centrifuge tubes and mixed based on equal numbers of cells during each time of medium change. The CMs were processed according to the MLEFF strategy with minor modifications (Weng et al. 2016b). In brief, the collected CMs were centrifuged at 500 g for 5 min to remove cells and cell debris. The supernatant was supplemented with 1% (v/v) protease inhibitor cocktail additive and filtrated through a 0.22 µm filter unit (Merck, Germany), then concentrated and desalted with water via Amicon 3 kDa filter devices (Merck, Germany). The concentrated CMs were processed with a protein equalization kit (ProteoMiner, Bio-Rad, CA) according to the published protocols (Weng et al. 2016b). Then, the "equalized" protein sample was separated with a GELFrEE 8100 Fractionation System (Expedeon, CA) according to the manufacturer's protocol, and ten fractions were subsequently collected. Each fraction was processed with a filter-aided sample preparation (FASP) method and the digested peptides were obtained through centrifugation and dried in a Speed Vac Concentrator (Thermo, MA).

LC-MS/MS analysis

The peptides were analyzed with a nano-RPLC-MS/MS on a Q-Exactive MS (Thermo, CA) coupled with an Ultimate



Database searching

The raw data were uploaded into Proteome Discoverer (PD, version 1.4.1.14) with Mascot (2.3.2) and were searched against the UniProtKB human complete proteome sequence database (release 2017 06, 24,148 entries). The reverse sequences were appended for an FDR evaluation (Wang et al. 2017b). The mass tolerances were set at 0.5 Da for the parent ions and at 10 ppm for the fragments. The peptides were searched using tryptic cleavage constraints, and a maximum of two missed cleavages were allowed. The minimal peptide length was six amino acids. Carbamidomethylation (C, +57.0215 Da) was used as the fixed modification. Oxidation (M, +15.9949 Da) and acetylation (protein N-termini, +42.0106 Da) were searched as variable modifications. Two SILAC-based labels, (Lys4, +4.0251 Da) and (Lys8, +8.0142 Da), were used as variable modification. The peptide and protein identifications were filtered by PD to keep the FDR \leq 1%. At least one unique peptide was required for each protein identification.

Bioinformatic analysis

The Gene Ontology (GO) annotation and Kyoto Encyclopedia of Genes and Genomes (KEGG) signaling pathway analysis were performed using DAVID 6.8 (https://david.ncifcrf.gov).



Production of recombinant Sika S100A4

The protein was expressed by Escherichia coli BL21 (DE3), and the expression was inducted with 0.3 mM IPTG. The recombinant GST-S100A4 protein was purified from the cell extract using glutathione agarose (Sigma) and cleaved with PreScission Protease (GE Healthcare; USA).

Proliferation assay

Cells were seeded at a density of $2-5\times10^3$ /well in a 96-well plate. Various concentrations of recombinant sika S100A4 (10 ng/ml, 100 ng/ml, 1 ug/ml) were added to different wells and made the final volume up to 200 μ l. At each time point (24, 48 h), cells were incubated in medium containing 20 μ l MTT/well for 4 h. Dimethyl sulfoxide (150 μ l; DMSO, Sigma, USA) was added to solubilize the formazan crystals and the OD value was read at 490 nm using an enzyme linked immunosorbent assay reader (TECAN; Grodig, Austria).

Tube formation

The tube formation assay was performed as previously described (Malinda et al. 1999). Briefly, Matrigel matrix with reduced growth factor was prepared according to manufacturer's advice (BD Biosciences); Fifty μ l of matrigel was add to each well of 96-well plates and allowed to gel for 30 min at 37°C. HUVECs (1.5×10⁴ cells) were suspended in 0.2 ml of the culture medium (containing 0 ng or 100 ng S100A4) and seeded into each well. Tube formation was observed under an inverted microscope 6 h later. At least five representative fields were viewed.

Results

Validation of the DPCs and DPC nodules

Morphology

The DPCs at their growth phase were typically stellate or spindle-shaped (Fig. 1a). After becoming confluent, DPCs started to condense and form multilayered aggregates (Fig. 1b), which ultimately formed evenly-distributed nodules (Fig. 1c). Therefore, in our culture system we had successfully induced the DPCs to form nodules, a phenotype that resembles the hair papillae in vivo.

Molecular attributes

Immunohistochemistry showed that almost all singularcultured DPCs stained positive for vimentin, α -SMA and VEGF (Fig. 1d), suggesting that the characteristics of the DPCs were maintained at the molecular level (Rufaut et al. 2013); all the DPC nodules stained positive for Versican and alkaline phosphatase (Fig. 1e), whereas the DPCs that did not participate in aggregate formation were negative. Since alkaline phosphatase and Versican are markers for DPC aggregates of hair follicles in vivo (Kishimoto et al. 1999; Rendl et al. 2005), our singular-culture system for DPCs had successfully mimicked the in vivo state.

Response of DPCs in nodule size to lithium chloride (LiCI)

LiCl at the concentration of 10 mM, 20 mM and 30 mM induced a dose-dependent reduction in DPC nodule size (Fig. 2). The nodules at 10 mM LiCl were significantly smaller than those at 0 mM (P < 0.01); at 20 mM significantly smaller than those at 10 mM (P < 0.01); and at 30 mM significantly smaller (essentially disappeared at this concentration) than those at 20 mM (P < 0.01). Therefore, the cultured DPCs had maintained their original characteristics as they still effectively responded to LiCl in a dose-dependent manner (Rufaut et al. 2013).

Validation of the co-culture system

Morphology

In the co-culture group, the DPCs began to aggregate to form observable nodules 5–7 days after the initial seeding for culture. Comparative analysis showed that the size of the DPC nodules formed in the co-culture group was significantly smaller (P < 0.01) and the number of nodules significantly fewer (P < 0.01) than those in the singular-culture group respectively (Fig. 3).

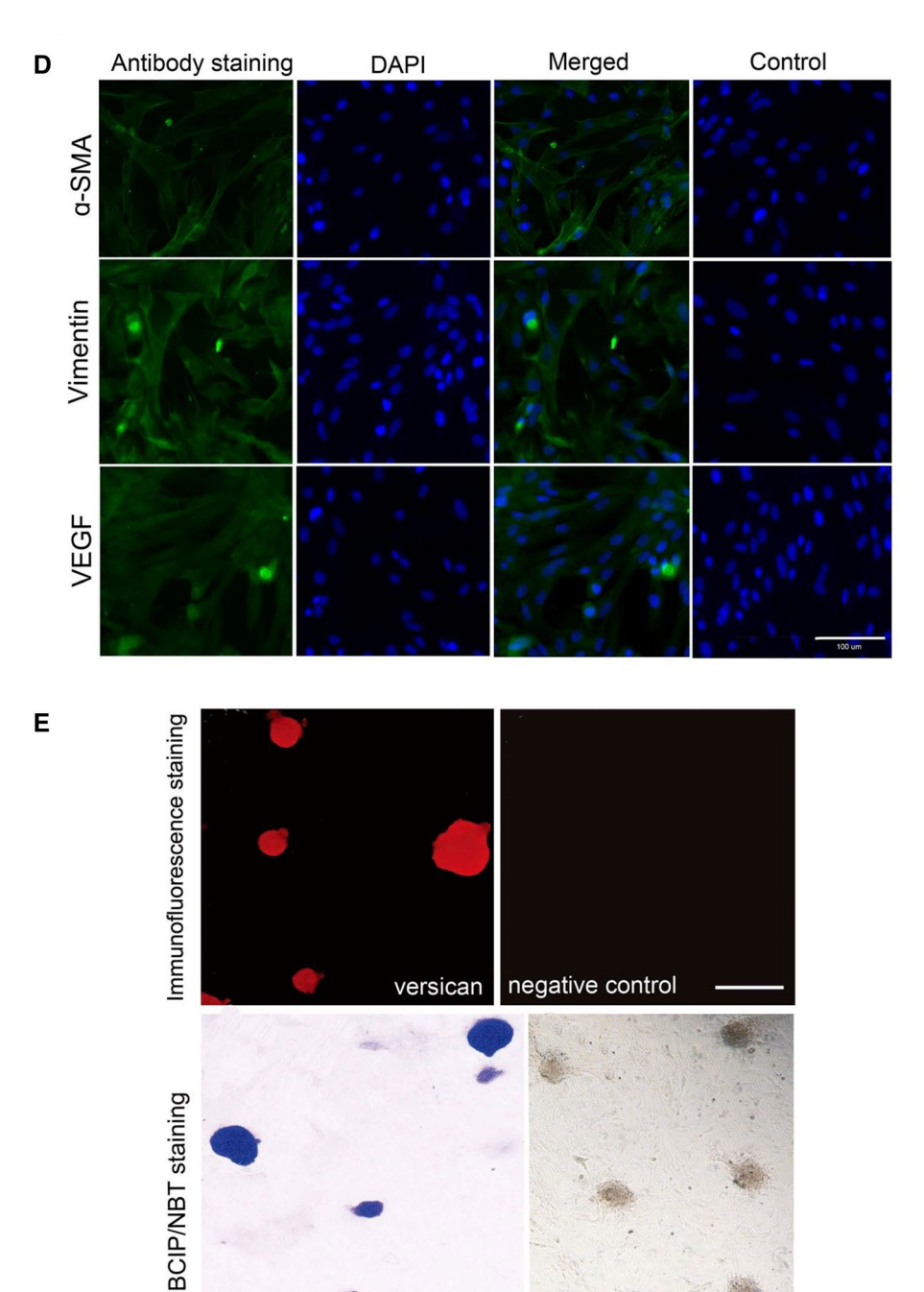
Effects of the co-culturing with the DPCs on the gene expression in the ASCs

To validate the co-culture system at the transcriptional level, we investigated the effects of the interactions between the DPCs and the ASCs on the expression of Nanog, Klf4 and Dkk3 genes in the ASCs. Results showed that expression levels of these three genes in the co-cultured ASCs were significantly down-regulated (P < 0.01) compared to those of the singular-culture (Fig. 4). Since Nanog, Klf4 and Dkk3 are three key embryonic stem cell genes (de Wilde et al. 2010; Shimasue et al. 2015; Takahashi and Yamanaka 2006; Wang et al. 2015) and that these genes were also found to be highly expressed in the singular-cultured ASCs (H and J 1974; Li and Suttie 2003; Li et al. 2009b), strongly



Fig. 1 Characterization of DP cells and DPC nodules. a Sub-confluent DPCs. Note that they were typically stellate or spindle shaped. b Condensed DPCs. Note that these DPCs formed multilayered aggregates. c Evenly-distributed nodules formed from the multilayered DPC aggregates. Phase contrast. Bar = 200 um in **a**, **b** and **c**. **d** Immunofluorescent staining of α-SMA, Vimentin, VEGF in singular-cultured DPCs. Almost all DPCs were stained positive for α -SMA, vimentin and VEGF, respectively. Bar = 100 um. e Characterization of DPC nodules. Immunofluorescent staining of versican viewed under UV light. DPC nodules were positively stained with antibody against versican. BCIP/NBT staining of endogenous alkaline phosphatase viewed with phase contrast. Positive staining of endogenous alkaline phosphatase was observed in whole nodules. Bars = 200 um





suggest that co-culture with the DPCs has induced ASCs to differentiate.

Reduction in nodule size and nodule number of the DPCs, and down-regulation in the expression level of stem cell

specific-genes in the co-cultured ASCs compared to those in the singular-cultured ones also strongly suggest that our coculture system had successfully mimicked the in vivo state.

alkaline phosphatase negative control



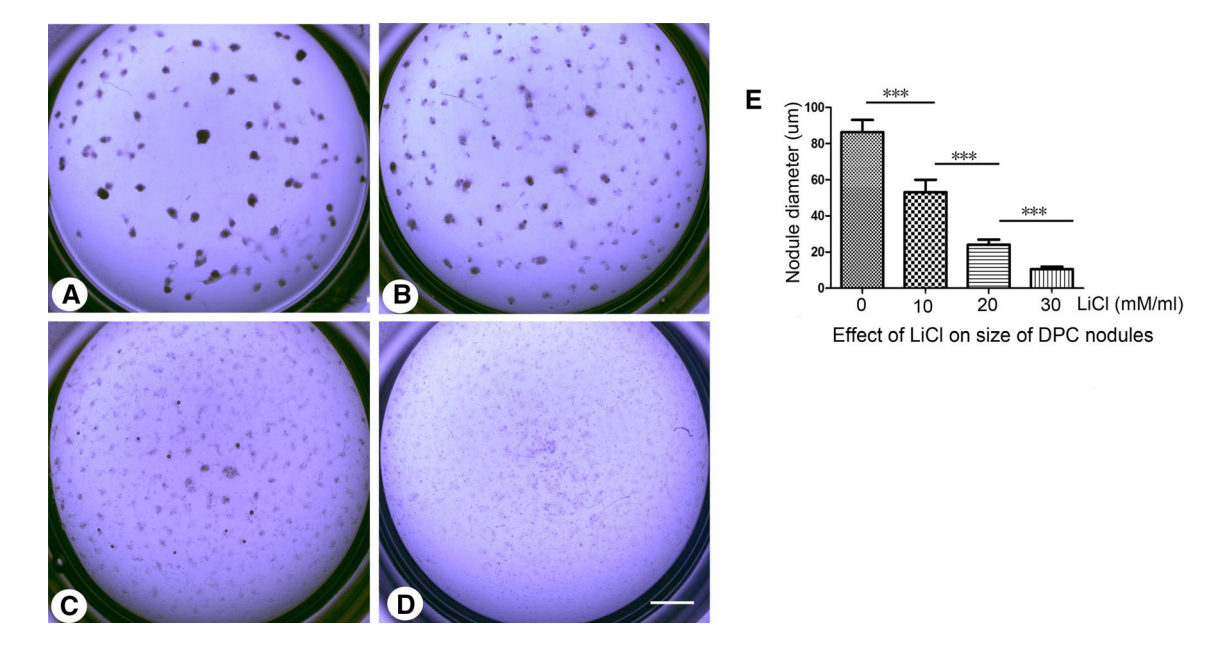


Fig. 2 Effects of LiCl on the size of DPC nodules. **a–d** Addition of lithium chloride (LiCl) at concentration of 0, 10, 20 and 30 mM respectively induced a dose-dependent reduction in size of DPC nodules. Bar=200 um. **e** Analysis of nodule diameter. Note that DPC nodules in the medium containing 10 mM LiCl were significantly smaller than those containing 0 mM LiCl; the nodules in 20 mM LiCl

were significantly smaller than those containing 10 mM LiCl; and the nodules in 30 mM LiCl were significantly smaller than those containing 20 mM LiCl, and were essentially disappeared at this concentration. *** $P \le 0.001$, error bars denote SD. Representative data is from three independent experiments

Identification of differentially expressed proteins (DEPs) from the co-cultured group

In total, 203 SILAC-labelled DEPs in the CMs from the coculture group were identified and subsequently quantified. Of the 203 DEPs, 128 were selected based on the following criteria: $\log_2(\text{SILAC ratio})$ is greater than 1.5 or less than -1.5 and with t test P-value less than 0.05 (n=3) (Table 1). Ninety-four of the 128 DEPs were selected from the comparison between the co-culture and the ASC singular-culture groups; 55 selected from the comparison between the coculture and the DPC singular-culture groups; and 21 were found to co-exist in both comparisons.

To put these 128 DEPs in a biological context, Gene Ontology (GO) analysis was used to classify them into three distinctive functional sets: Cellular component, Molecular function and Biological process (Fig. 5). In the "Cellular component", 18 GO terms were enriched, these DEPs were mainly located in the extracellular exosome, focal adhesion, extracellular matrix, extracellular region, and extracellular space (Fig. 5a). In the "Molecular function", 13 GO terms were enriched. The mostly enriched term was binding, such as protein binding, poly(A) RNA binding, heparin binding, calcium ion binding, actin binding, extracellular matrix binding, collagen binding, unfolded protein binding, ECM structural constituent, cadherin binding involved in cell–cell adhesion, and double-stranded RNA binding (Fig. 5b). In the "Biological process", 22 GO

terms were enriched, and the most abundant ones were protein folding, positive regulation of gene expression, collagen fibril organization, and cell–cell adhesion (Fig. 5c). Other GO terms that were enriched and worth noting are regulation of cell growth, osteoblast differentiation, and angiogenesis (Fig. 5c).

In total, 13 KEGG pathways were enriched (P<0.001) from the dataset using DAVID software (Fig. 6). The most significant KEGG pathways for the DEPs were focal adhesion (16 proteins), ECM-receptor interaction (9 proteins) and PI3K-Akt signaling pathway (16 proteins).

Functional analysis of one of the DEPs, S100A4, in vitro

S100A4 was expressed and purified, and then, its functions were analyzed. Our results showed that both 100 ng/ml and 1ug/ml S100A4 significantly increased the proliferation rate of HUVECs (Fig. 7a; p < 0.05). S100A4 at the concentration of 100 ng/ml significantly stimulated the tube formation of HUVECs compared with the control (Fig. 7b, c; p < 0.01). Therefore, S100A4 has a strong angiogenic activity.



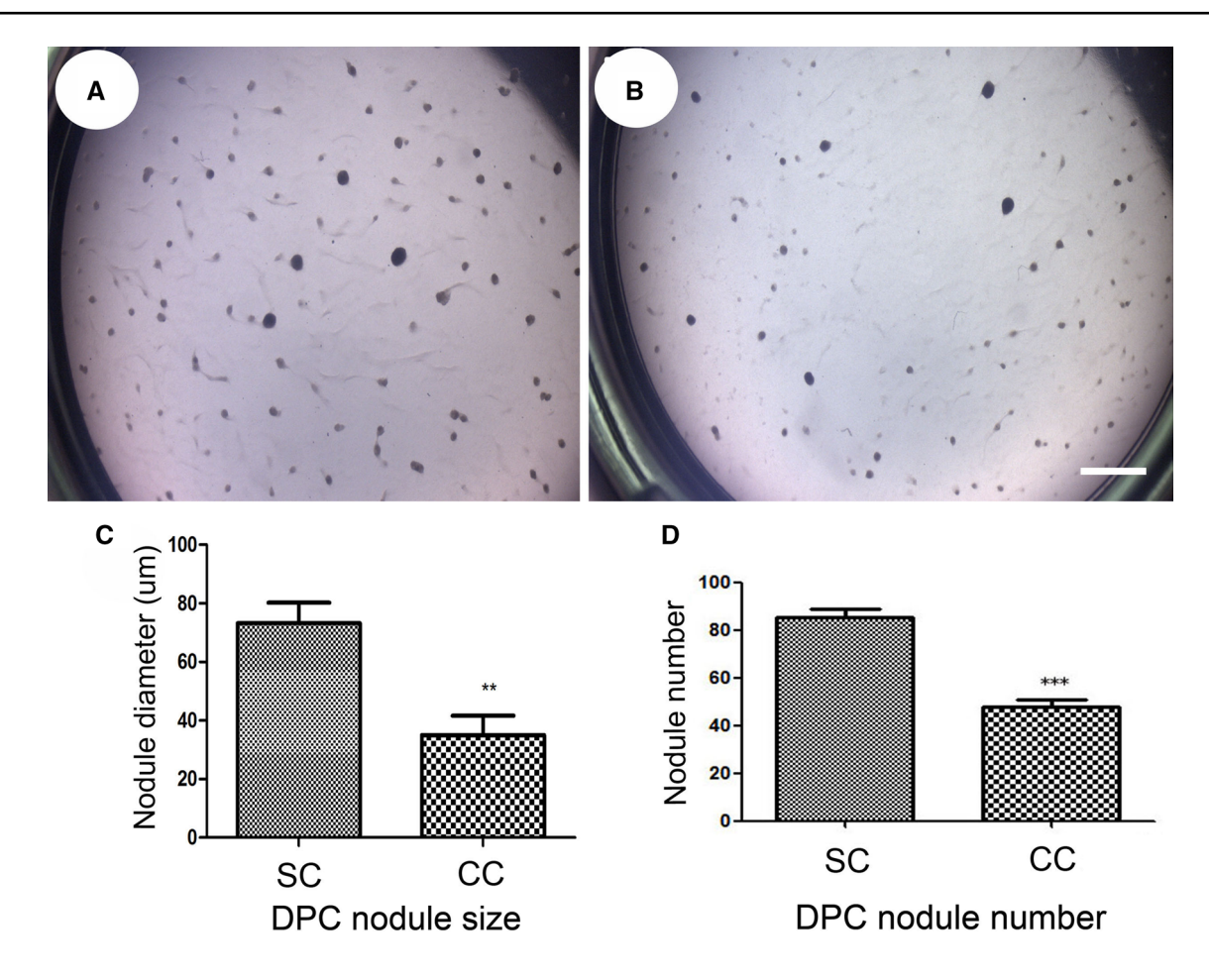


Fig. 3 Changes in DPC nodule parameters between singular-culture and co-culture. **a** DPC nodules in the singular-culture. **b** DPC nodules in the co-culture between the ASCs and DPCs. **c** Diameter analysis of DPC nodules. Note that diameter of the DPC nodules was significantly smaller in the co-culture than the ones in singular-culture.

d Number analysis of DPC nodules. Note that number of the DPC nodules were significantly less in the co-culture than the singular-culture. SC singular-culture; CC co-culture. Bar = 200 um. **P \leq 0.01, ***P \leq 0.001. error bars denote SD. Representative data is from three independent experiments

Discussion

In this study, we successfully established an in vitro cell coculture system that could effectively mimic the interactions between ASCs and DPCs (one of the two niche cell types) in vivo. Thus, we have significantly simplified the process for the identification and isolation of interactive molecules that may be involved in the differentiation of ASCs. Using this system, we identified candidate interactive molecules and key transduction pathways, which, we believe, may be the key signals for triggering the initiation of antler development. Identification of these molecules would undoubtedly help us to gain insights into the mechanism of antler development and renewal, the only case of stem cell-based full regeneration of a mammalian organ.

Antler generation/regeneration rely on the presence of stem cells, i.e. ASCs (Li 2012; Li et al. 2013, 2014), triggered by interactions between the ASCs (APs/PPs) and their niche, i.e. the closely associated skin (Li 2012). Interactions

between the ASCs and niche cell types may be realized through exchanging diffusible molecules, since interposition of an impermeable membrane between ASCs and the skin in vivo abrogates antler generation, whereas a semipermeable membrane (pore size: $0.45~\mu m$) delays, but cannot stop antler formation (Li et al. 2007, 2008). However, these interactive molecules are still elusive due to the complexity of the in vivo state, which has greatly hindered progress on revealing the molecular mechanism of antler formation/regeneration.

In the present study, we took an in vitro approach and established a co-culture system based on the interactions between ASCs and DPCs. In this system, the size and number of nodules of DPCs in the co-culture group were significantly reduced compared with the singular-cultured group. We know that antler generation/regeneration are accompanied with transition of skin type from scalp/pedicle skin to velvet skin (Deb-Choudhury et al. 2015; Li and Suttie 2000). And that the distribution density of hair follicles and



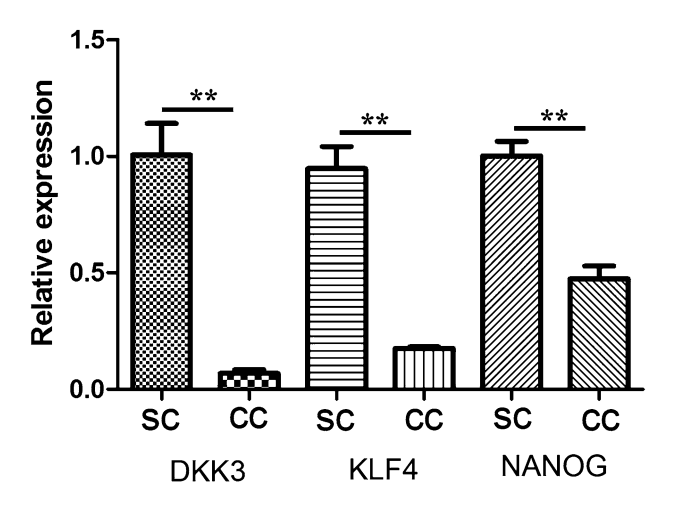


Fig. 4 Changes in gene expression level of NANOG, KLF4 and DKK3 in the ASCs between singular-culture and co-culture. Gene expression level of NANOG, KLF4 and DKK3 in the ASCs in the co-culture (CC) were down-regulated significantly compared to the singular-culture (SC). ** $P \le 0.01$. error bars denote SD. Representative data is from three independent experiments

thickness of hair shafts in velvet skin are significantly lower/ smaller than those in scalp/pedicle skin (Li et al. 2013). Classical studies show that formation of each hair follicle in vivo is induced by a DPC aggregate and the diameter of a hair shaft is in direct proportion to the size of that DPC aggregate (Rufaut et al. 2006). Hence, our co-culture system has successfully mimicked the in vivo state at the morphological level. Furthermore, three stem cell marker genes, Nanog, klf4, DKK3, were significantly down-regulated in the co-cultured ASCs compared to singular-cultured ASCs. It is reported that expression of these three marker genes is closely correlated with the degree of stemness of stem cells (Wang et al. 2016). Down-regulation of these genes in the ASCs in the co-culture group means that the ASCs must have started to loss their stemness and begun to differentiate after the interaction with the co-cultured DPCs. We know that upon establishment of the interactions between the ASC tissue and the enveloping skin during antler development, the ASCs begin to differentiate toward the osteogenic lineage and gradually lose their stem cell attributes (Le Bihan et al. 2012; Li et al. 2005; Raimondo et al. 2017). Therefore, our co-culture system has successfully mimicked the in vivo state at the molecular level. The successful establishment of this novel co-culture system has allowed us to pursue studies on the identification of the elusive interactive molecules for antler generation/regeneration.

Although the in vitro approach is considered to be the most powerful way to identify and isolate the proteins that mediate complex biological phenomenon in vivo (Bowler and Merryman 2015; Raimondo et al. 2017; Weinreb and Nemcovsky 2015), these low abundant proteins are normally

masked by the much more abundant serum proteins in the culture medium. For example, in a typical cell culture (1×10 ⁷ cells cultured for 24 h) experiment, around 20–80 μg of secreted proteins could be released into the medium across different cell types (Hsu et al. 2014; Le Bihan et al. 2012), in which the concentration of serum proteins could reach ~ 60 mg/ml (Weng et al. 2016b). In order to overcome this problem, Weng et al. developed an efficient method called MLEFF (Weng et al. 2016a, b). In their method, SILAC label is introduced to distinguish the cellular proteins from those of the FBS background. Thereafter, a protein equalization technique was used to reduce the dynamic range of the proteins in the CM sample. Protein fractionation was then applied to decrease the complexity of the samples and provide more likelihood for identifying the targeted lowabundant-proteins. This approach enabled sensitive, highthroughput, reproducible, and unbiased secretome identification and analysis to be carried out.

In the present study, the approach of MLEFF was adopted to analyze the CMs collected from our co-culture system. In total, 128 SILAC-labeled proteins were found to be altered at the expression level. Most of these proteins were extracellular-located proteins, over 60% of which belonged to the extracellular exosome function in the Cellular component through GO analysis. Therefore, the MLEFF approach had worked in our study for the identification of secreted proteins from the medium containing FBS. These results strongly suggest interactions that occurred between the ASCs and DPCs in our co-culture system may have facilitated the release of exosomal proteins, as the main means of cell–cell communication.

Antler generation/regeneration are stem cell-based processes, where activation of ASCs drives them to proliferate and differentiate toward the osteogenic lineage. In the present study, we found that both secreted frizzled-related protein 1 (SFRP1) and dickkopf-3 (DKK-3) were significantly downregulated in ASCs in the co-cultured group compared to the singular-cultured group (Table 1). Interestingly, both of these molecules are potent inhibitors of the Wnt signaling pathway through direct interaction with Wnt proteins (Kong et al. 2017). SFRP1 inhibits Wnt signaling pathway through decreasing the intracellular beta-catenin level (Kong et al. 2017; Liu et al. 2018a; Wang et al. 2017c). The Wnt pathway has previously been shown to play a role in stimulating osteogenic differentiation (Yuan et al. 2016). Further studies show that SFRP1 can inhibit osteogenic differentiation of mouse bone marrow stem cell (BMSCs) likely through down-regulating the Wnt signaling pathway (Luo et al. 2018). Therefore, during initiation of antler growth in vivo, inhibitors of Wnt signaling (such as SFRP1 and DKK-3) must be down-regulated in ASCs to activate Wnt signaling, which then drives the ASCs to differentiate toward the osteogenic lineage and to form bony antlers.



 Table 1
 Differentially expressed proteins (DEPs)

Accession no	Protein name	Gene name	Ratio (Log2)	T-test sig- nificant	P-value
Q17QP5	Secreted frizzled-related protein 4 SFRP1	SFRP1	- 3.296	+	0.005
A6QL81	DKK3 protein DKK3	DKK3	- 2.922	+	0.019
F1MG02	Extracellular matrix protein 2 ECM2	ECM2	- 2.908	+	0.021
F1MQX1	Uncharacterized protein SRPX	SRPX	- 2.638	+	0.004
G3N0V0	Uncharacterized protein (fragment)		- 2.593	+	0.022
A5LIP3	Carboxy peptidase PPCA	PPCA	- 2.545	+	0.047
P14769	N-acetyllactosaminide alpha-1,3- galactosyltransferase GGTA1	GGTA1	-2.534	+	0.008
F1MZ40	Uncharacterized protein (fragment) GAS6	GAS6	-2.303	+	0.013
A7YY58	LTBP1 protein LTBP1	LTBP1	- 2.113	+	0.006
Q0VCX1	Complement C1s subcomponent C1S	C1S	-2.100	+	0.047
Q08E54	Amyloid beta (A4) protein APP	APP	- 1.986	+	0.051
E1BI02	Fibromodulin	FMOD	- 1.931	+	0.034
Q0P569	Nucleobindin-1	NUCB1	- 1.908	+	0.019
G3X745	Glypican-1	GPC1	- 1.871	+	0.046
Q28022	Microfibrillar-associated protein 5	MFAP5	- 1.790	+	0.012
Q95121	Pigment epithelium-derived factor PEDF	SERPINF1	- 1.780	+	0.030
Q3T0I2	Pro-cathepsin H CTSH	CTSH	- 1.739	+	0.042
Q5BIP2	Platelet-derived growth factor receptor-like protein PDGFRL	PDGFRL	- 1.720	+	0.006
F1MJH1	Gelsolin GSN	GSN	- 1.634	+	0.012
F1N1C7	Uncharacterized protein AEBP1	AEBP1	- 1.600	+	0.002
J9QDG1	Periostin variant 3		- 1.592	+	0.048
F1N430	Metalloproteinase inhibitor 2 TIMP2	TIMP2	- 1.579	+	0.023
E1BLS8	Uncharacterized protein EMILIN1	EMILIN1	- 1.534	+	0.028
Q3T148	Eukaryotic translation initiation factor 3 subunit M EIF3M	EIF3M	- 2.201	+	0.003
E1BA17	Uncharacterized protein COL14A1	COL14A1	- 1.951	+	0.001
F1MXS8	Collagen alpha-1(III) chain COL3A1	COL3A1	- 1.799	+	0.007
B8Y9S9	Embryo-specific fibronectin 1 transcript variant Fibronectine FN1	FN1	- 1.575	+	0.042
P02453	Collagen alpha-1(I) chain COL1A1	COL1A1	- 1.532	+	0.027
F1N0K0	Collagen alpha-1(XI) chain	COL11A1	- 1.501	+	0.013
P48616	Vimentin VIM	VIM	1.500		0.013
A2VE41	EGF-containing fibulin-like extracellular matrix protein 1	EFEMP1	1.516	+	0.011
F1MTP5	WD repeat-containing protein 1	WDR1	1.581	+	0.003
				+	0.002
Q3ZC84	Cytosolic non-specific dipeptidase	CNDP2	1.652	+	
A1L517	FK506 binding protein 9 (Fragment)	FKBP9	1.661	+	0.019
A5D7J6	CALR protein	CALR	1.662	+	0.029
P19120	Heat shock cognate 71 kDa protein	HSPA8	1.672	+	0.032
A6QLY8	IGFBP7 protein	IGFBP7	1.686	+	0.007
G3MYJ0	Uncharacterized protein		1.725	+	0.024
A5PKA3	CCDC80 protein	CCDC80	1.735	+	0.052
Q76LV2	Heat shock protein HSP 90-alpha	HSP90AA1	1.741	+	0.001
Q5KR47-2	Isoform 2 of Tropomyosin alpha-3 chain	TPM3	1.744	+	0.003
P62261	14-3-3 protein epsilon YWHAE	YWHAE	1.768	+	0.009
F1N3A1	Thrombospondin-1 THBS1	THBS1	1.814	+	0.000
Q76LV1	Heat shock protein HSP 90-beta	HSP90AB1	1.830	+	0.016
Q0VCX2	78 kDa glucose-regulated protein	HSPA5	1.861	+	0.027
Q2KJH6	Serpin H1	SERPINH1	1.895	+	0.033
F1MAZ4	Uncharacterized protein (fragment)	CHRDL1	1.903	+	0.004
Q3ZBN5	Asporin	ASPN	1.935	+	0.034
B0JYN3	L-lactate dehydrogenase	LDHB	1.955	+	0.009



 Table 1 (continued)

Accession no	Protein name	Gene name	Ratio (Log2)	T-test sig- nificant	P-value
Q5E9A1	Nascent polypeptide-associated complex subunit alpha	NACA	1.956	+	0.005
G5E5C3	Proteasome subunit alpha type	PSMA6	2.012	+	0.006
Q08E18	HDGF protein	HDGF	2.030	+	0.002
Q3ZBY4	Fructose-bisphosphate aldolase	ALDOC	2.101	+	0.001
Q58CQ2	Actin-related protein 2/3 complex subunit 1B	ARPC1B	2.130	+	0.005
F1MEN8	Protein disulfide-isomerase A4	PDIA4	2.143	+	0.015
Q5E9B7	Chloride intracellular channel protein 1	CLIC1	2.207	+	0.022
P60712	Actin, cytoplasmic 1	ACTB	2.230	+	0.008
A7MB62	Actin-related protein 2	ACTR2	2.270	+	0.051
G3X757	Transitional endoplasmic reticulum ATPase	VCP	2.319	+	0.001
A6H7J6	Protein disulfide-isomerase	P4HB	2.360	+	0.002
F1MUP9	Uncharacterized protein	VAT1	2.361	+	0.011
Q3SZ54	Eukaryotic initiation factor 4A-I	EIF4A1	2.376	+	0.022
E1BFV0	Uncharacterized protein	KPNB1	2.377	+	0.010
A1XEA0	Elongation factor 1 alpha (fragment)	EEF1A1	2.383	+	0.005
P61157	Actin-related protein 3	ACTR3	2.419	+	0.002
A6QNL5	PDIA6 protein (fragment)	PDIA6	2.424	+	0.034
Q862I9	Similar to acidic ribosomal phosphoprotein PO (fragment)		2.468	+	0.043
M0QVZ4	Lysyl oxidase homolog 2	LOXL2	2.478	+	0.026
A6QLL8	Fructose-bisphosphate aldolase	ALDOA	2.480	+	0.005
Q3T148	Eukaryotic translation initiation factor 3 subunit M	EIF3M	2.489	+	0.024
F1MB08	Alpha-enolase	ENO1	2.553	+	0.009
P53619	Coatomer subunit delta	ARCN1	2.632	+	0.003
A7Z057	14-3-3 protein gamma	YWHAG	2.633	+	0.002
Q27971	Calpain-2 catalytic subunit	CAPN2	2.639	+	0.002
A5D7D1	Alpha-actinin-4	ACTN4	2.668	+	0.020
Q3MHR7	Actin-related protein 2/3 complex subunit 2	ARPC2	2.710	+	0.020
Q3B7N2	Alpha-actinin-1	ACTN1	2.738	+	0.031
Q3B7N2 Q3SYU2	Elongation factor 2	EEF2	2.783	+	0.031
Q33102 Q17QZ9	Interferon-induced protein with tetratricopeptide repeats 5	IFIT5	2.786		0.040
F6RWK1		ARHGAP1	2.852	+	0.003
	Uncharacterized protein	CSPG4		+	
F1MY84	Uncharacterized protein		2.878	+	0.032
P62157	Calmodulin	CALM	2.962	+	0.015
Q3ZCI4	6-phosphogluconate dehydrogenase, decarboxylating	PGD	3.003	+	0.049
P19858	L-lactate dehydrogenase A chain	LDHA	3.015	+	0.011
A6QR28	Phosphoserine aminotransferase	PSAT1	3.029	+	0.030
A0JNP1	SMC1A protein	SMC1A	3.051	+	0.029
F1MHV8	Calponin-2 (Fragment)	CNN2	3.121	+	0.040
A5D984	Pyruvate kinase	PKM2	3.177	+	0.023
F1MQ37	Uncharacterized protein	МҮН9	3.268	+	0.025
Q5KR49	Tropomyosin alpha-1 chain	TPM1	3.286	+	0.000
Q3SZI2	Lamin A/C	LMNA	3.337	+	0.012
Q3MHL3	Histone-binding protein RBBP4	RBBP4	3.422	+	0.053
F1N169	Uncharacterized protein	FLNA	3.552	+	0.012
A6QR15	LOC535277 protein	LOC535277	3.705	+	0.001
Q9TS87	Transgelin	TAGLN	3.916	+	0.028
Q3B7M5	LIM and SH3 domain protein 1	LASP1	3.920	+	0.002
Q0QES8	Glyceraldehyde-3-phosphate dehydrogenase (fragment)	GAPDH	4.021	+	0.002
A2VDN8	Coronin	CORO1C	4.023	+	0.039



 Table 1 (continued)

Accession no	Protein name	Gene name	Ratio (Log2)	T-test sig- nificant	P-value
Q3T0P6	Phosphoglycerate kinase 1	PGK1	4.169	+	0.031
A2VE99	Septin-11	SEPT11	4.649	+	0.011
E1BFV0	Uncharacterized protein	KPNB1	1.506	+	0.016
A6QLL8	Fructose-bisphosphate aldolase	ALDOA	1.550	+	0.028
Q2KHU8	Eukaryotic translation initiation factor 2 subunit 3	EIF2S3	1.594	+	0.002
F1N169	Uncharacterized protein	FLNA	1.606	+	0.046
A5D7D1	Alpha-actinin-4	ACTN4	1.607	+	0.018
Q9TQT8	Interferon-gamma (fragment)		1.609	+	0.005
F1MPU0	Clathrin heavy chain 1 (fragment)	CLTC	1.618	+	0.014
P61157	Actin-related protein 3	ACTR3	1.627	+	0.003
Q3SYU2	Elongation factor 2	EEF2	1.643	+	0.022
F2Z4E7	Uncharacterized protein	ILF2	1.647	+	0.003
A2VE99	Septin-11	SEPT11	1.708	+	0.025
Q0QES8	Glyceraldehyde-3-phosphate dehydrogenase (fragment)	GAPDH	1.715	+	0.046
P21282	V-type proton ATPase subunit C 1	ATP6V1C1	1.716	+	0.016
Q5E9A1	Nascent polypeptide-associated complex subunit alpha	NACA	1.723	+	0.016
P35466	Protein S100-A4	S100A4	1.727	+	0.000
Q862I9	Similar to acidic ribosomal phosphoprotein PO (Fragment)		1.751	+	0.029
A6H767	Nucleosome assembly protein 1-like 1	NAP1L1	1.752	+	0.044
F1N6U4	Uncharacterized protein	SEPT9	1.761	+	0.015
Q3ZCI4	6-phosphogluconate dehydrogenase, decarboxylating	PGD	1.771	+	0.039
Q3SZI2	Lamin A/C	LMNA	1.785	+	0.005
A5D973	Alpha isoform of regulatory subunit A, protein phosphatase 2	PPP2R1A	1.786	+	0.029
F1MQ37	Uncharacterized protein	МҮН9	1.790	+	0.024
Q28019	Latent-transforming growth factor beta-binding protein 2	LTBP2	1.802	+	0.004
P61286	Polyadenylate-binding protein 1	PABPC1	1.806	+	0.020
Q0V8C0	Platelet-derived growth factor receptor-like protein (fragment)	PDGFRL	1.850	+	0.047
Q58CQ2	Actin-related protein 2/3 complex subunit 1B	ARPC1B	1.857	+	0.002
A7MB62	Actin-related protein 2	ACTR2	1.868	+	0.002
Q76LV2	Heat shock protein HSP 90-alpha	HSP90AA1	1.907	+	0.006
Q3SYU6	Calponin-2	CNN2	1.931	+	0.049
A2VDN8	Coronin	CORO1C	1.949	+	0.050
O08DI9	Matrix metallopeptidase 19	MMP19	1.969	+	0.030
Q5E949		HRMT1L2	1.980		0.034
F1MDC1	HMT1 hnRNP methyltransferase-like 2 isoform 3			+	
G5E531	Uncharacterized protein	RRBP1	2.010	+	0.046
	T-complex protein 1 subunit alpha	TCP1	2.032	+	0.010
G3X757	Transitional endoplasmic reticulum ATPase	VCP	2.077	+	0.030
G3X6Q8	Pentraxin-related protein PTX3	PTX3	2.188	+	0.042
Q05443	Lumican	LUM	2.244	+	0.006
G3MYJ0	Uncharacterized protein	****	2.329	+	0.012
F1MUP9	Uncharacterized protein	VAT1	2.376	+	0.002
A5D9H5	Heterogeneous nuclear ribonucleoprotein D	HNRPD	2.660	+	0.048
Q862H8	Similar to 40S ribosomal protein SA (P40) (fragment)		2.711	+	0.012
Q2KJ47	EH-domain containing 2	EHD2	2.790	+	0.025
Q27971	Calpain-2 catalytic subunit	CAPN2	2.817	+	0.035
F1MC48	Uncharacterized protein	IQGAP1	2.902	+	0.028
Q07130	UTPglucose-1-phosphate uridylyltransferase	UGP2	3.038	+	0.026
F1MWD3	Uncharacterized protein	CCT5	3.344	+	0.042
F1MV66	Uncharacterized protein	OAS1Y	3.397	+	0.003



T. I. I. 4	/ · · · 1\
Table 1	(continued)

Accession no	Protein name	Gene name	Ratio (Log2)	T-test sig- nificant	P-value
Q0QEM9 Q8HZY1	ATP synthase subunit beta (fragment) Serine protease inhibitor clade E member 2	ATP5B SERPINE2	3.546 5.738	+ +	0.001 0.038

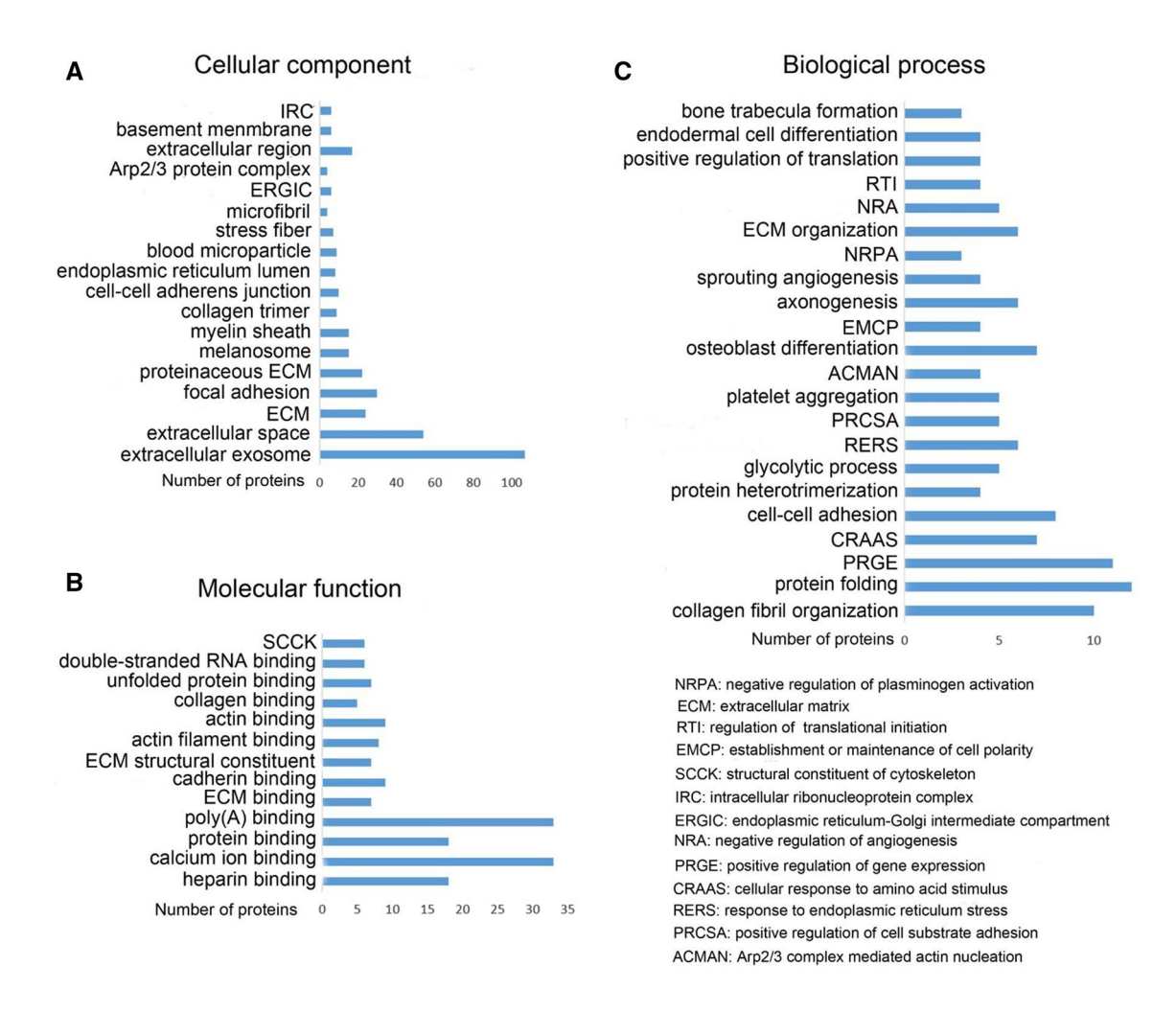


Fig. 5 Enriched gene ontology (GO) terms using DAVID analysis. GO analysis to the identified DEPs using DAVID analysis. Only are the terms that had p-value \leq 0.01 shown. a cell component, b molecular function, c biological process

Regenerating deer antlers are the fastest growing mammalian tissue (exceeds 2 cm/day) (Goss and Rosen 1973), which undoubtedly requires ample blood supply. In the present study, a number of molecules related to angiogenesis were identified from the co-culture system. The expression of a number of potent angiogenic factors, such as \$100A4, Hepatoma Derived Growth Factor (HDGF); and ATP synthase subunit beta (ATP5B), were significantly up-regulated; whereas, a number of anti-angiogenic factors, such as Pigment epithelium-derived factor (PEDF), thrombospondin-1 (THBS1), thrombospondin-2 (THBS2) and secreted protein

acidic and rich in cysteine (SPARC), were significantly down-regulated in the co-cultured group compared to the singular-cultured group (Table 1). S100A4 is an 11-kD protein, one of the members of the S100 protein family. Previous study showed that this molecule was specifically located in blood vessel walls in the vascularized tissues of the pre-cartilage zone in the growing antlers, suggesting that S100A4 might play a role in angiogenesis. Our studies showed that S100A4 significantly stimulated proliferation and tube formation of HUVECs. So, the function of S100A4 on angiogenesis was further determined in vitro. HDGF is



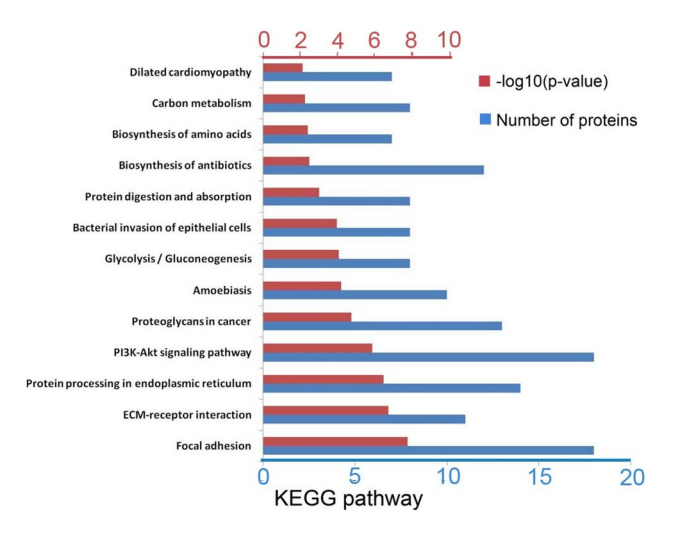
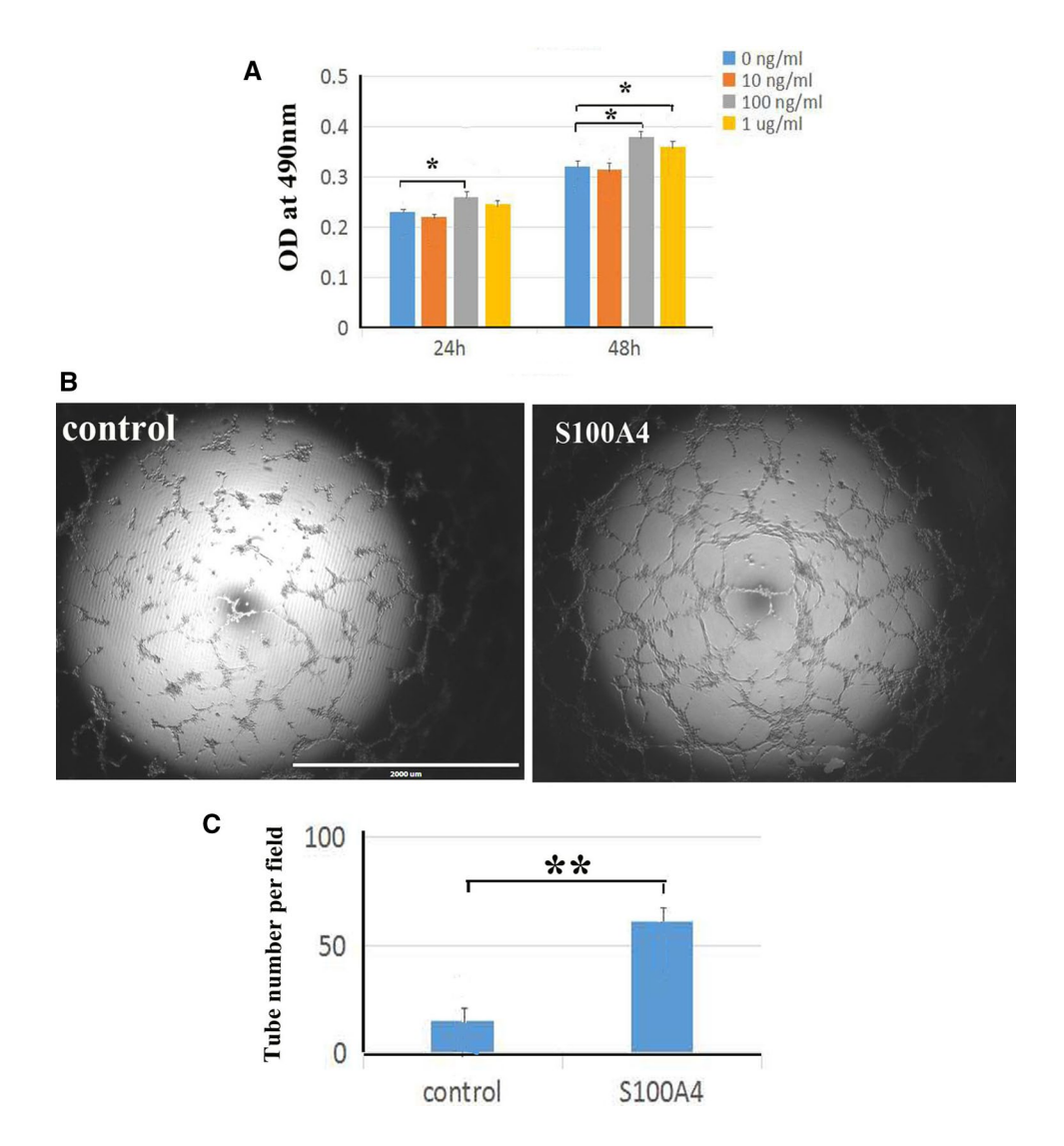


Fig. 6 Distribution of KEGG Pathways participated by the DEPs. Enriched pathways from the dataset using DAVID software. Only are the pathways that had p-value ≤ 0.01 shown

a secreted mitogen, which is significantly expressed in the nucleus of smooth muscle and endothelial cells, hence, highly associated with blood vessel formation, particularly in tumors (Everett and Bushweller 2003). ATP5B is a mitochondrial ATP synthase, involved in energy production and closely related to endothelial cell function (Xu and Li 2016), such as significant promotion of angiogenesis in the CAM assay (Ochiya et al. 2014). Studies also show that ATP5B plays a key role in proliferation, migration, and tube formation of HUVECs (Wang et al. 2017a). Hence, it can be considered an important regulator of angiogenesis (Greening et al. 2015).

Angiogenesis during antler generation/regeneration could also be further promoted by the down-regulation of anti-angiogenic factors. Down-regulated anti-angiogenic factors detected in our co-culture system were PEDF, THBS1, THBS2 and SPARC. PEDF is a secreted protein and consists of 418 amino acids. A 34-mer fragment of PEDF (residues 24–57) was shown to have anti-angiogenic

Fig. 7 Angiogenic activity of S100A4 protein on HUVECs in vitro. a MTT proliferation assay. Dose-response effects of S100A4 on the proliferation of HUVECs. The most effective dosage was found to be 100 ng/ml at 24 and 48 h. The data, mean \pm SD; *p < 0.05, significantly different from the control. b Tube formation assay. S100A4 (100 ng/ml) significantly increased number of loops from HUVECs. Bar = 2000 μ m. c Bar graph to quantify the results of loop numbers. Numbers of loops were counted using ImageJ software. All controls in the figure were negative control (without addition of any growth factor). The data, mean \pm SD; **p<0.01, significantly different from the control





properties (Loegl et al. 2016; Zhang et al. 2016). PEDF mRNA was detected in most cell/tissue types in the antler growth centre except vascular cells (Lord et al. 2007), suggesting that PEDF may not be directly involved in blood vessel formation in antler growth. Both thrombospondins (THBS1 & 2) and SPARC are known to be downstream anti-angiogenic proteins and are upregulated by PEDF (Phan et al. 2007). Therefore, down-regulation of PEDF would inevitably inhibit expression of the thrombospondins and SPARC genes.

Studies have shown that syntheses of the extracellular matrix in DPCs was significantly increased in the aggregative growth pattern than in the non-aggregative growth pattern (Jinjin et al. 2004). Collagens (COLs) are the main components (25–35%) of extracellular matrix, and are mainly involved in the process of extracellular matrix structure and extracellular matrix binding (Theocharis et al. 2016). There are a dozen types of COLs in living animals, of which COL-1 is the main type (90%) (Di Lullo et al. 2002). In this study, we found that four types of COL (COL1A1, COL3A1, COL11A1, COL14A1) and Fibronectin 1 protein in the CM were down-regulated significantly in the co-culture group compared to those in the singular-culture group. At the same time, the ability of aggregative growth of DPCs was decreased in the co-culture group. Therefore, our co-culture system had effectively impaired the ability of DPC aggregation, which might be through regulation of COL secretion. Again, the results from our co-culture system are consistent with the findings from the in vivo state.

In our previous studies, we have demonstrated that the PI3K-AKT signaling pathway is predominantly involved in the initiation of antler development (Liu et al. 2018b). It is known that PI3K-AKT signaling plays key roles in regulating cell cycle progression, cell proliferation, differentiation and migration (King et al. 2015; Peltier et al. 2007), and can be activated by many different types of upstream stimulators, including growth hormones, cytokines, and extra cellular matrix proteins(Man et al. 2003). In our present study, we detected significant up-regulation of Hsp90AB and Hsp90AA in the co-culture group compared to the singularculture group, and these HSP proteins could have directly activated the PI3K-AKT signaling pathway, and then initiation of antler formation. In addition, up-regulation of the YWHAG protein in the PI3K-AKT signaling pathway may also contribute to cell proliferation, angiogenesis, and DNA repair of the ASCs. As the fastest proliferating cell type, ASCs would require a potent means of DNA repair mechanism to avoid becoming cancerous. Recently using comparative genome approaches, Wang et al. found some positively selected genes (e.g., FOS, REL, FAM83A, PML, NMT2) for fast proliferating and neoplastic inhibiting in antler system. These genes together with our findings should be taken into consideration when pursue this line of study.

In conclusion, in this study, we established an in vitro cell co-culture model, which was then validated at both the morphological and molecular levels. Functional testing experiments demonstrated that this system could successfully mimic the in vivo state. Therefore, we have significantly simplified the process to identify interacting molecules between ASCs and DPCs. Moreover, we adopted the MLEFF strategy, to include the SILAC method, which had enabled us to effectively eliminate the high-abundant-protein background from FBS, and identified meaningful molecules and transduction pathways. We believe this work has laid the foundation for the eventual discovery of the molecules that mediate the interactions between the ASCs and niche cell types for antler generation/regeneration.

Acknowledgments The authors like to thank Eric Lord for carefully reading through the manuscript. This research was funded by The Strategic Priority Research Program of the Chinese Academy of Sciences (Grant Number XDA16010105), National key research and development program (Grant Number 2018YFC1706603-03), The National Natural Science Fund of China (Grant Number 31500792).

Compliance with Ethical Standards

Conflict of interest The authors declare no conflict of interest.

References

- Bowler MA, Merryman WD (2015) vitro models of aortic valve calcification: solidifying a system Cardiovascular pathology: the official journal of the Society for. Cardiovasc Pathol 24:1–10. https://doi.org/10.1016/j.carpath.2014.08.003
- Chunyi Li A, Yang F, Suttie J (2011) Stem cells, stem cell niche and antler development. Anim Prod Sci 51:267–276
- de Wilde J, Hulshof MF, Boekschoten MV, de Groot P, Smit E, Mariman EC (2010) The embryonic genes Dkk3, Hoxd8, Hoxd9 and Tbx1 identify muscle types in a diet-independent and fiber-type unrelated way. BMC Genomics 11:176. https://doi.org/10.1186/1471-2164-11-176
- Deb-Choudhury S, Wang W, Clerens S, McMahon C, Dyer JM, Li C (2015) Direct localisation of molecules in tissue sections of growing antler tips using MALDI imaging. Mol Cell Biochem 409:225–241. https://doi.org/10.1007/s11010-015-2527-7
- Di Lullo GA, Sweeney SM, Korkko J, Ala-Kokko L, San Antonio JD (2002) Mapping the ligand-binding sites and disease-associated mutations on the most abundant protein in the human type I collagen. J Biol Chem 277:4223–4231. https://doi.org/10.1074/jbc.m110709200
- Everett AD, Bushweller J (2003) Hepatoma derived growth factor is a nuclear targeted mitogen. Curr Drug Targets 4:367–371. https://doi.org/10.2174/1389450033490975
- Goss RJ (1995) Future directions in antler research. Anat Record 241:291–302. https://doi.org/10.1002/ar.1092410302
- Goss RJ, Powel RS (1985) Induction of deer antlers by transplanted periosteum. I. Graft size and shape. J Exp Zool 235:359–373. https://doi.org/10.1002/jez.1402350307
- Goss RJ, Rosen JK (1973) The effect of latitude and photoperiod on the growth of antlers. J Reprod Fertil Suppl 19:111–118



- Greening DW et al (2015) Molecular profiling of cetuximab and bevacizumab treatment of colorectal tumours reveals perturbations in metabolic and hypoxic response pathways. Oncotarget 6:38166–38180. https://doi.org/10.18632/oncotarget.6241
- Harper A, Wang W, Li C (2009) Identifying ligands for S100A4 and galectin 1 in antler stem cells. Queenstown molecular biology meetings. The Queenstown Molecular Biology Meeting Society Inc:Q35
- Hartwig H, Schrudde J (1974) Experimentelle Untersuchungen zur Bildung der primaren Stirnauswuchse beim Reh (*Capreolus capreolus* L.). Z Jagdwiss 20:13
- Hsu C-W, Yu J-S, Peng P-H, Liu S-C, Chang Y-S, Chang K-P, Wu C-C (2014) Secretome profiling of primary cells reveals that THBS2 is a salivary biomarker of oral cavity squamous cell carcinoma. J Proteome Res 13:4796–4807
- Jinjin W, Yuangang L, Tangyou Z, Wei L, Rongqing L (2004) Determination of proliferation and collagen synthesis of human dermal hair papilla cells. J Clin Dermatol 33:3
- King D, Yeomanson D, Bryant HE (2015) PI3King the lock: targeting the PI3K/Akt/mTOR pathway as a novel therapeutic strategy in neuroblastoma. J Pediatr Hematol/Oncol 37:245–251. https://doi.org/10.1097/mph.0000000000000329
- Kishimoto J, Ehama R, Wu L, Jiang S, Jiang N, Burgeson RE (1999) Selective activation of the versican promoter by epithelial- mesenchymal interactions during hair follicle development. Proc Natl Acad Sci USA 96:7336–7341
- Kong LY, Xue M, Zhang QC, Su CF (2017) In vivo and in vitro effects of microRNA-27a on proliferation, migration and invasion of breast cancer cells through targeting of SFRP1 gene via Wnt/beta-catenin signaling pathway. Oncotarget 8:15507– 15519. https://doi.org/10.18632/oncotarget.14662
- Le Bihan MC et al (2012) In-depth analysis of the secretome identifies three major independent secretory pathways in differentiating human myoblasts. J Proteomics 77:344–356. https://doi.org/10.1016/j.jprot.2012.09.008
- Li C (2012) Deer antler regeneration: a stem cell-based epimorphic process. Birth Defects Res Part C 96:51–62. https://doi. org/10.1002/bdrc.21000
- Li C, Suttie JM (2000) Histological studies of pedicle skin formation and its transformation to antler velvet in red deer (*Cervus elaphus*). Anat Record 260:62–71
- Li C, Suttie JM (2003) Tissue collection methods for antler research. Eur J Morphol 41:23–30
- Li C, Suttie JM, Clark DE (2005) Histological examination of antler regeneration in red deer (*Cervus elaphus*). Anat Record Part A 282:163–174. https://doi.org/10.1002/ar.a.20148
- Li C et al (2007) Antler regeneration: a dependent process of stem tissue primed via interaction with its enveloping skin. J Exp Zool Part A 307:95–105. https://doi.org/10.1002/jez.a.352
- Li C, Yang F, Xing X, Gao X, Deng X, Mackintosh C, Suttie JM (2008) Role of heterotypic tissue interactions in deer pedicle and first antler formation-revealed via a membrane insertion approach. J Exp Zool Part B 310:267–277. https://doi.org/10.1002/jez.b.21210
- Li C et al (2009a) Development of a nude mouse model for the study of antlerogenesis—mechanism of tissue interactions and ossification pathway Journal of experimental zoology Part B. Mol Dev Evol 312:118–135. https://doi.org/10.1002/jez.b.21252
- Li C, Yang F, Sheppard A (2009b) Adult stem cells and mammalian epimorphic regeneration-insights from studying annual renewal of deer antlers. Curr Stem Cell Res Therapy 4:237–251
- Li C et al (2010) Stem cells responsible for deer antler regeneration are unable to recapitulate the process of first antler development-revealed through intradermal and subcutaneous tissue transplantation. J Exp Zool Part B 314:552–570. https://doi.org/10.1002/jez.b.21361

- Li C, Pearson A, McMahon C (2013) Morphogenetic mechanisms in the cyclic regeneration of hair follicles and deer antlers from stem cells. BioMed Res Int 2013:643601. https://doi. org/10.1155/2013/643601
- Li C, Zhao H, Liu Z, McMahon C (2014) Deer antler–a novel model for studying organ regeneration in mammals. Int J Biochem Cell Biol 56:111–122. https://doi.org/10.1016/j.biocel.2014.07.007
- Liu J et al (2018a) Methylation of secreted frizzled-related protein 1 (SFRP1) promoter downregulates Wnt/beta-catenin activity in keloids. J Mol Histol 49:185–193. https://doi.org/10.1007/s10735-018-9758-3
- Liu Z, Zhao H, Wang D, McMahon C, Li C (2018b) Differential effects of the PI3K/AKT pathway on antler stem cells for generation and regeneration of antlers in vitro. Front Biosci (Landmark edn) 23:1848–1863
- Loegl J et al (2016) Pigment epithelium-derived factor (PEDF): a novel trophoblast-derived factor limiting feto-placental angiogenesis in late pregnancy. Angiogenesis 19:373–388. https://doi.org/10.1007/s10456-016-9513-x
- Lord EA, Martin SK, Gray JP, Li C, Clark DE (2007) Cell cycle genes PEDF and CDKN1C in growing deer antlers. Anat Record 290:994–1004. https://doi.org/10.1002/ar.20562
- Luo Y, Zhang Y, Miao G, Zhang Y, Liu Y, Huang Y (2018) Runx1 regulates osteogenic differentiation of BMSCs by inhibiting adipogenesis through Wnt/beta-catenin pathway. Arch Oral Biol 97:176–184. https://doi.org/10.1016/j.archoralbio.2018.10.028
- Malinda KM et al (1999) Identification of laminin alpha1 and beta1 chain peptides active for endothelial cell adhesion, tube formation, and aortic sprouting. FASEB J 13:53–62
- Man HY et al (2003) Activation of PI3-kinase is required for AMPA receptor insertion during LTP of mEPSCs in cultured hippocampal neurons. Neuron 38:611–624
- Ochiya T, Takenaga K, Endo H (2014) Silencing of S100A4, a metastasis-associated protein, in endothelial cells inhibits tumor angiogenesis and growth. Angiogenesis 17:17–26. https://doi.org/10.1007/s10456-013-9372-7
- Peltier J, O'Neill A, Schaffer DV (2007) PI3K/Akt and CREB regulate adult neural hippocampal progenitor proliferation and differentiation. Dev Neurobiol 67:1348–1361. https://doi.org/10.1002/dneu.20506
- Phan E, Ahluwalia A, Tarnawski AS (2007) Role of SPARC-matricellular protein in pathophysiology and tissue injury healing. Implications for gastritis and gastric ulcers. Med Sci Monit 13:RA25-RA30
- Raimondo JV et al (2017) Methodological standards for in vitro models of epilepsy and epileptic seizures A TASK1-WG4 report of the AES/ILAE translational task force of the ILAE. Epilepsia 58(Suppl 4):40–52. https://doi.org/10.1111/epi.13901
- Rendl M, Lewis L, Fuchs E (2005) Molecular dissection of mesenchymal-epithelial interactions in the hair follicle. PLoS Biol 3:e331. https://doi.org/10.1371/journal.pbio.0030331
- Rj G (1987) Induction of deer antlers by transplanted periosteum. II. Regional competence for velvet transformation in ectopic skin. J Exp Zool Part A 244:101–111
- Rolf HJ et al (2008) Localization and characterization of STRO-1 cells in the deer pedicle and regenerating antler. PLoS ONE 3:e2064. https://doi.org/10.1371/journal.pone.0002064
- Rufaut NW, Goldthorpe NT, Wildermoth JE, Wallace OA (2006) Myogenic differentiation of dermal papilla cells from bovine skin. J Cell Physiol 209:959–966. https://doi.org/10.1002/jcp.20798
- Rufaut NW, Nixon AJ, Goldthorpe NT, Wallace OA, Pearson AJ, Sinclair RD (2013) An in vitro model for the morphogenesis of hair follicle dermal papillae. J Invest Dermatol 133:2085–2088. https://doi.org/10.1038/jid.2013.132
- Shimasue A, Yamakawa N, Watanabe M, Hidaka Y, Iwatani Y, Takano T (2015) Expression analysis of stemness genes in a rat thyroid



- cell line FRTL5. Exp Clin Endocrinol Diabetes 123:48–54. https://doi.org/10.1055/s-0034-1389924
- Sun H, Yang F, Chu W, Zhao H, McMahon C, Li C (2012) Lentiviral-mediated RNAi knockdown of Cbfa1 gene inhibits endochondral ossification of antler stem cells in micromass culture. PLoS ONE 7:e47367. https://doi.org/10.1371/journal.pone.0047367
- Takahashi K, Yamanaka S (2006) Induction of pluripotent stem cells from mouse embryonic and adult fibroblast cultures by defined factors. Cell 126:663–676. https://doi.org/10.1016/j.cell.2006.07.024
- Theocharis AD, Skandalis SS, Gialeli C, Karamanos NK (2016) Extracellular matrix structure. Adv Drug Deliv Rev 97:4–27. https://doi.org/10.1016/j.addr.2015.11.001
- Wang HW et al (2015) Discovering monotonic stemness marker genes from time-series stem cell microarray data. BMC Genomics 16(Suppl 2):S2. https://doi.org/10.1186/1471-2164-16-s2-s2
- Wang D, Guo Q, Ba H, Li C (2016) Cloning and characterization of a Nanog pseudogene in Sika Deer (*Cervus nippon*). DNA Cell Biol 35:576–584. https://doi.org/10.1089/dna.2016.3303
- Wang DT, Chu WH, Sun HM, Ba HX, Li CY (2017a) Expression and functional analysis of tumor-related factor S100A4 in antler stem cells. J Histochem Cytochem 65:579–591. https://doi. org/10.1369/0022155417727263
- Wang M, Tian F, Ying W, Qian X (2017b) Quantitative proteomics reveal the anti-tumour mechanism of the carbohydrate recognition domain of Galectin-3 in Hepatocellular carcinoma. Sci Rep 7:5189. https://doi.org/10.1038/s41598-017-05419-5
- Wang Z, Jia Y, Du F, Chen M, Dong X, Chen Y, Huang W (2017c) IL-17A inhibits osteogenic differentiation of bone mesenchymal stem cells via Wnt signaling pathway. Med Sci Monitor 23:4095–4101

- Weinreb M, Nemcovsky CE (2015) vitro models for evaluation of periodontal wound healing/regeneration. Periodontology 2000(68):41–54. https://doi.org/10.1111/prd.12079
- Weng Y, Sui Z, Shan Y, Hu Y, Chen Y, Zhang L, Zhang Y (2016a) Effective isolation of exosomes with polyethylene glycol from cell culture supernatant for in-depth proteome profiling. The Analyst 141:4640–4646. https://doi.org/10.1039/c6an00892e
- Weng Y et al (2016b) In-depth proteomic quantification of cell secretome in serum-containing conditioned medium. Anal Chem 88:4971–4978. https://doi.org/10.1021/acs.analchem.6b00910
- Xu G, Li JY (2016) ATP5A1 and ATP5B are highly expressed in glioblastoma tumor cells and endothelial cells of microvascular proliferation. J Neuro-Oncol 126:405–413. https://doi.org/10.1007/ s11060-015-1984-x
- Yuan Z et al (2016) PPARgamma and Wnt signaling in adipogenic and osteogenic differentiation of mesenchymal stem cells. Curr Stem Cell Res Therapy 11:216–225
- Zhang H et al (2016) PEDF and 34-mer inhibit angiogenesis in the heart by inducing tip cells apoptosis via up-regulating PPAR-gamma to increase surface FasL. Apoptosis 21:60–68. https://doi.org/10.1007/s10495-015-1186-1

Publisher's Note Springer Nature remains neutral with regard to jurisdictional claims in published maps and institutional affiliations.

